TECTONICS, VOL. 21, NO. 3, 1018, 10.1029/2001TC001339, 2002

Modeling the evolution of the Guadalquivir foreland basin (southern Spain)

D. Garcia-Castellanos,[1] M. Fernàndez, and M. Torne

Institute of Earth Sciences, Jaume Almera, Consejo Superior de Investigaciones Científicas (CSIC), Barcelona, Spain

Received 5 February 2001; revised 23 November 2001; accepted 29 November 2001; published 25 June 2002.

[1] Previous quantitative studies dealing with the origin of foreland basins have focused primarily either on the rheological basis of the lithosphere mechanical response or on the relationship between orogenic loading and sediment geometry. To link the evolution of the Guadalquivir foreland basin (South Iberia) with the thermomechanical stratification of the Iberian lithosphere, we combine quantitative approaches to deep and shallow processes: thrust loading, lithospheric flexure, thickness changes of the crust and the lithospheric mantle, and surface mass transport. A planform flexural analysis of the present-day load distribution shows that basement subsidence is related not only to upper crustal thrusting but also to a deep-seated additional load. On the basis of the observed gravity and geoid fields, we propose this additional load to be related to a lithospheric mantle thickening larger than the coeval crustal thickening. Further modeling of the evolution of a basin cross section reveals that the architecture of the sedimentary basin is additionally related to the lithosphere rheological response. The quantitative study of the evolution of basement faulting and the forebulge uplift of Sierra Morena leads us to conclude that viscous stress relaxation and/or plastic yielding within the lithosphere are key processes to explain the flexural evolution of the basin. *INDEX TERMS:* 8105 Tectonophysics: Continental margins and sedimentary basins; 8102 Tectonophysics: Continental contractional orogenic belts; 8120 Tectonophysics: Dynamics of lithosphere and mantle—general; 8122 Tectonophysics: Dynamics, gravity and tectonics; 8158 Tectonophysics: Evolution of the Earth: Plate motions—present and recent (3040); *KEYWORDS:* lithospheric flexure, anelastic rheology, basin architecture, hidden load, Betic Range, Sierra Morena

1. Introduction

[2] The lithosphere retains finite strength on geological timescales when submitted to external loads, behaving as a rigid thin plate resting on a fluid asthenosphere. Foreland basins have been interpreted as sedimentary accumulations occurring on continental lithosphere when this is tectonically loaded and flexed by an orogenic wedge. Therefore the geometry of the sedimentary infill is expected to be strongly dependent not only on the tectonic evolution of the orogen but also on the rheological behavior of the lithosphere during flexure.

[3] Many authors have studied the evolution of foreland basins by using numerical methods to quantitatively link the processes of orogenic growth, erosion/sedimentation, and flexure. *Beaumont* [1981] used a viscoelastic plate model to simulate the flexural response of the lithosphere in the Alberta Basin. *Flemings and Jordan* [1989] incorporated wedge-progradation gradual loading and sedimentation. Later, *Toth et al.* [1996] and *Ford et al.* [1999] explicitly related loading with thrusting in the active margin of the sub-Andean foreland and the western Alps, respectively. Many among these and other works found that the load derived from the present topography or the thrust kinematics cannot satisfactorily explain the basement deflection. The required additional load [e.g., *Royden and Karner*, 1984; *Bott*, 1991], sometimes referred as "hidden load," is found to be both positive [e.g., *Brunet*, 1986; *Royden*, 1988] or negative [*Lyon-Caen and Molnar*, 1983, 1985] according to the region of study. This load has been interpreted in diverse ways such as the effect of a relevant paleobathymetry prior to the formation of topography [*Stockmal et al.*, 1986; *Van der Beek and Cloetingh*, 1992] or the effect of subcrustal forces such as slab pull [*Royden and Karner*, 1984].

[4] Simultaneously, several authors used synthetic approaches to study the detailed mechanical response of the lithosphere. It has been repeatedly shown that anelastic behavior of the oceanic lithosphere modifies its flexural deflection pattern [e.g., *Bodine et al.*, 1981; *Garcia-Castellanos et al.*, 2000]. The equivalent implications of the rheological layering for continental flexure were studied by *McNutt et al.* [1988] and *Burov and Diament* [1992, 1995] among others. *Waschbusch and Royden* [1992] related the episodicity during the evolution of foreland basins to the flexural effects of elastic-plastic yielding in the lithosphere. However, there is a lack of modeling studies integrating both surface (erosion/sedimentation) and deep (lithospheric scale) processes to reproduce the evolution of foreland basins.

[5] The work presented here intends to show that integrating the quantitative modeling of the lithosphere anelastic behavior and the thrust load evolution and incorporating simple approaches of noninstantaneous ero-

[1]Now at Faculty of Earth Sciences, Vrije Universiteit, Amsterdam, Netherlands.

0278-7407/02/2001TC001339$12.00

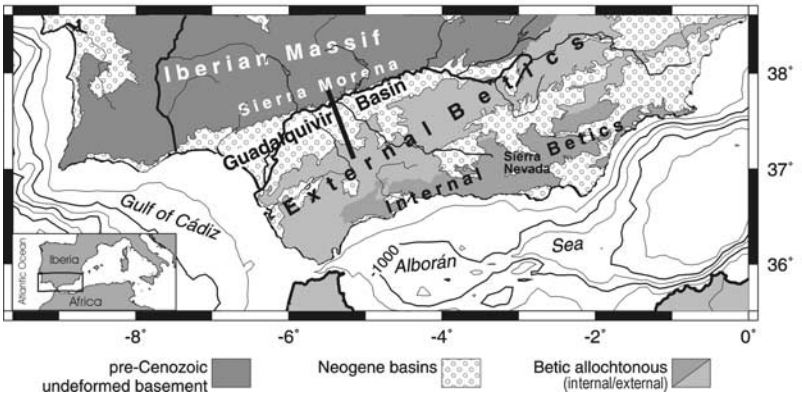

Figure 1. Geological map of the Guadalquivir Basin. Major rivers and bathymetry isolines (every 500 m) are shown. The bold line indicates the cross section modeled in this work.

sion/sedimentation can provide new insights into the system as a whole. In particular, we propose a self-consistent quantitative model for the evolution of the Guadalquivir Basin (southern Spain) linking the emplacement of the Betic Range, the subcrustal mass redistribution, and the rheology of the flexed lithosphere. For this purpose, we apply a numerical code based on *Garcia-Castellanos et al.* [1997] that allows the calculation of the flexural subsidence of a multilayered lithosphere (in a similar way to *Waschbusch and Royden* [1992] and *Burov and Diament* [1992, 1995]) when loaded by noninstantaneous thrusting and erosion/sedimentation processes (similar to *Toth et al.* [1996]).

[6] Previous flexural modeling of the Guadalquivir foreland basin [*Van der Beek and Cloetingh*, 1992] showed that the present-day basement depth is explained by loading of an elastic plate only if an extra load is added to the topographic load. Subsequently, the flexural origin of the basin has been adopted to interpret various observations such as stress measurements [*Herraiz et al.*, 1996] or refraction seismics [*González et al.*, 1998]. Recent seismic, oil well, heat flow, palaeontological, and field data compilations and interpretations by *Fernàndez et al.* [1998a], *Berástegui et al.* [1998], and *Sierro et al.* [1996] provide the keys to model the basin evolution, linking it with the structure and mechanical behavior of the south Iberian lithosphere and permitting identification of the different loads and evaluation of their timing.

2. Tectonic Setting

[7] The Neogene Guadalquivir foreland basin is located in the southern part of the Iberian Peninsula, limited by the Iberian Massif to the north and the Betic mountain chain to the south (Figure 1). The Betic Range is the northern segment of a strongly arcuate orogen that continues in the Rif Chain (northern Africa) across the Gibraltar Strait. The Alborán Sea extensional basin occupies at present the inner part of this orogen. The tectonic evolution of the whole area, which constitutes the westernmost part of the Alpine Chain, was controlled by the post-Cretaceous relative movement between the African and Eurasian plates. Plate motion studies from *Dewey et al.* [1989] suggest that this part of the plate boundary experienced ~200 km of roughly N-S convergence between mid-Oligocene and late Miocene, followed by ~50 km of WNW directed oblique convergence from late Miocene to Recent time.

[8] The major paleogeographic elements forming the Betics-Guadalquivir system correspond to three tectonic domains that were well delimited by the beginning of the Neogene [*Balanyá and Garčía-Dueñas*, 1987]: (1) the External Zones of the Betic chain corresponding to the inverted Mesozoic continental margin of the Iberian plate; (2) the Flysch Units, which are made up of allochthonous sediments; and (3) the Internal Zones of the Betic chain, composed of a polyphase thrust stack that includes three high-pressure low-temperature metamorphic nappe complexes [e.g. *Bakker et al.*, 1989; *Tubia and Gil-Ibarguchi*, 1991].

[9] The tectonic evolution of the Betic Range is relatively poorly constrained, and its study has lead to significant discrepancies between authors. For instance, *Platt* [1998] requires only two tectonic events (compressive and extensive) to explain the metamorphic record and other geological evidence, whereas *Balanyá et al.* [1997] define four tectonic events of successive compression and extension. There are also discrepancies on the depth of the contact between External and Internal Betics, varying from midcrustal [*Banks and Warburton*, 1991] to the base of crust [*Sanz de Galdeano*, 1990] and the base of lithosphere [*Montenat and D'Estevou*, 1996]. Similar disagreements arise regarding the age of the sedimentary infill of the Guadalquivir Basin, where the oldest Neogene sediments have been dated either as Helvetian [*Perconig*, 1962, 1971], Tortonian [*Sierro et al.*, 1996], or very late Langhian [*Berástegui et al.*, 1998; *Fernàndez et al.*, 1998a]. The basin infill records progradation toward the WSW after the Messinian [*Sierro et al.*, 1996], reflecting the present direction of sediment transport, whereas before this period the sedimentary units show small lateral variations along the strike of the basin [*Berástegui et al.*, 1998].

[10] Late Cretaceous and Palaeogene convergence caused crustal thickening in the Internal Zones and generated an

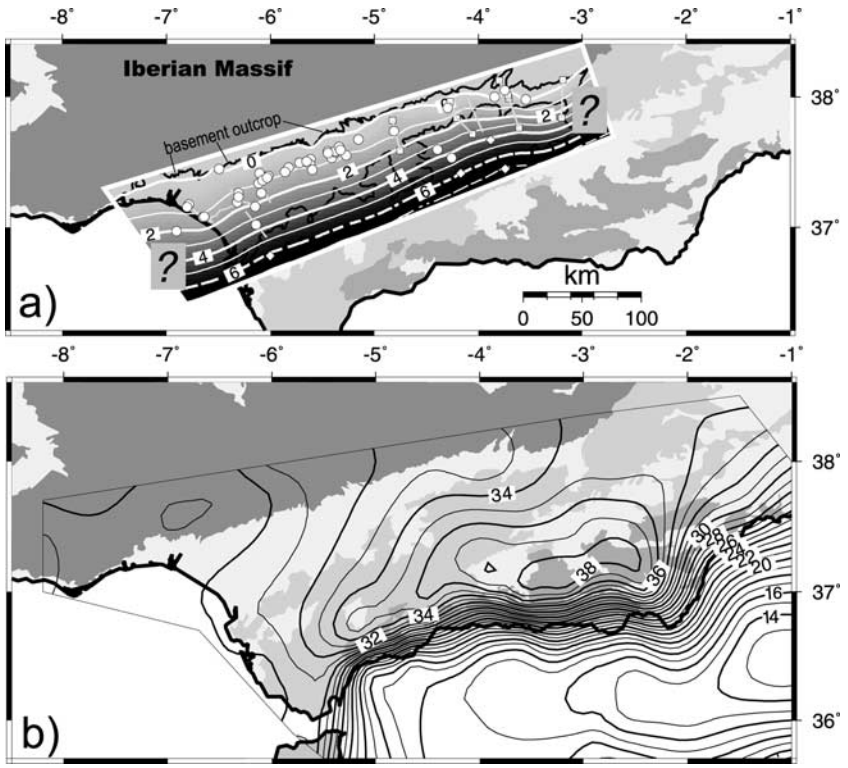

Figure 2. (a) Pre-Cenozoic undeformed basement depth compiled from oil wells (circles), seismic lines (squares), and geological cross sections (diamonds). Depth is in kilometers relative to the present-day sea level. Question marks indicate lack of reliability due to basement deformation (east) and lack of data (west). Modified from *Fernàndez et al.* [1998a]. (b) Moho depth (in kilometers) of the South Iberian region (modified from *Torne et al.* [2000]).

orogen by nappe stacking. Whether this thickening occurred in the present-day Alborán Sea basin or further to the east is still under debate. The Internal Zones represent the disrupted and extended fragments of this pre-Miocene orogen [*Balanyá and Garčía-Dueñas*, 1987; *Platt and Vissers*, 1989; *Platt et al.*, 1995; *Monié et al.*, 1991; *Vissers et al.*, 1995]. In contrast, the Betic External Zones and the Flysch Units reflect continued crustal shortening during Miocene, coeval with crustal extension occurring in the Internal Zones. This shortening began in the early Aquitanian (23 Ma) and continued into the late Miocene [*Garčía-Dueñas et al.*, 1992; *Comas et al.*, 1992]. The relative movement at the Internal-External Betics boundary is described by *Platzman* [1992] and *Platzman et al.* [1993] as a dextral rotation zone.

[11] Miocene extensional systems and fault-bounded sedimentary basins are superimposed upon the continental collision of the Internal Zones [e.g., *Galindo Zaldivar et al.*, 1989; *Garčía-Dueñas and Balanyá,* 1991; *Platt and Vissers*, 1989; *Garčía-Dueñas et al.*, 1992]. This Miocene extensional phase was accompanied by a distinctive low-pressure high-temperature metamorphism [*Zeck et al.*, 1992].

[12] In summary, the Guadalquivir Basin formed in an overall environment of plate convergence as the late foreland basin of the Betics, but this convergence is not reflected in the extensional Neogene kinematics of either the Internal Betic zones or the Alborán Basin. The present-day Guadalquivir Basin only correlates with the late stages (Langhian to Recent) of the Betic tectonic history that began during Late Cretaceous.

3. Data

[13] To quantitatively relate the basin infill of the Guadalquivir Basin to the emplacement of the Betic orogenic wedge and the mechanical behavior of the lithosphere, it must be determined both the sedimentary evolution of the basin and the present-day distribution of the load related to crustal thickness changes. We have considered as main constraints the depth to the top of the basement, the present-day crustal structure, and the geometry of the sedimentary infill.

3.1. Basement Depth

[14] The depth to the top of the undeformed pre-Cenozoic basement (Palaeozoic with an autochthonous Mesozoic cover at some places) has been compiled by *Fernàndez et al.* [1998a] from 44 oil wells, 10 commercial seismic profiles, and geological cross sections [*Banks and Warburton*, 1991]. Most of the wells are located in the basin except for three that are located on the External Betics. These three wells penetrate more than 3000 m of allochthonous Mesozoic carbonates. The basement depth (Figure 2a) is tilted

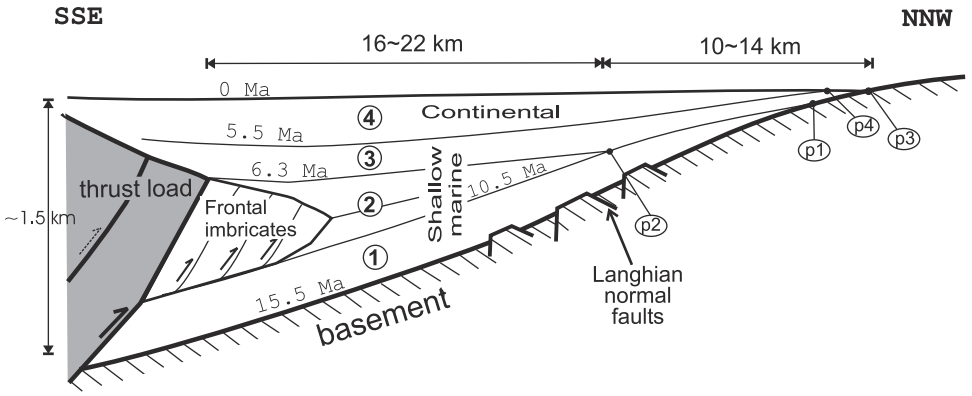

Figure 3. Synthesis of the geometry of the basin and its sedimentary infill based on the work by *Berástegui et al.* [1998], *Fernàndez et al.* [1998a], and *Sierro et al.* [1996]. Sedimentary units are as follows: 1, Latest Langhian-Serravallian; 2, Tortonian; 3, Messinian; 4, Plio-Quaternary. The pinch-outs of the units are indicated as p1, p2, p3, and p4. See location in Figure 1.

toward the SSE with increasing slope (from 2.5° to 6°) in the same direction and little variations along the strike (slight narrowing of the basin toward the ENE). The basement reaches depths of 5 km at a distance of only 60–80 km from the northern limit of the basin. The depositional environments during the early basin stages are reported as shallow, nearshore marine [*Berástegui et al.*, 1998], which indicates that the basement has undergone a considerable subsidence. This contrasts with the moderate present-day topography of the Betic orogen, suggesting that if the basin has a flexural origin, then thrust stacking in the upper crust was not the only loading mechanism. As depicted in commercial seismic lines, the basement is involved in normal faulting affecting the lowest part of the basin fill and, in some places, there is evidence of compressive reactivation of faults [*Fernàndez et al.*, 1998a].

3.2. Crustal Thickness

[15] The Moho depth map of the region (Figure 2b) is based on a compilation by *Fernàndez et al.* [1998a] from refraction and wide-angle seismic data and gravity modeling. Additionally, we incorporate several seismic lines from the ILIHA refraction survey, modeled by *González et al.* [1998], which provide more detail in the western side of Sierra Morena. The crustal thickness in the Iberian Massif is 31–33 km increasing toward the Central Betics, where the Moho reaches a maximum depth of ~38 km below the Central Betics and close to the maximum topography. The transition to the Alborán Sea is characterized by a very sharp crustal thinning occurring over a narrow band of 30–35 km width, following the shoreline [*Torne and Banda*, 1992]. The crustal thickness values in the Alborán Basin decrease radially toward the center and the east of the basin, ranging between 20 and 24 km in the western part and <12 km in the easternmost Alborán Basin [*Torne et al.*, 2000].

[16] Lateral variations in crustal thickness over the region reveal two notable features. First, *González et al.* [1998] reported a slight crustal thinning (of the order of 1 km) in the northern margin of the basin, below Sierra Morena (location in Figure 1). The lack of evidence for Neogene fault activity in this range suggests that the present relief of Sierra Morena (deeply river incised and with altitudes mostly ranging from 600 surely to 1000 m) and the slight rise of the Moho may be partially a consequence of flexural forebulge uplift. Second, it is worth noting that the Moho does not deepen toward the SSE as sharply as the autochthonous basement, indicating that the crustal thickness, excluding the Neogene sediments and the Betic allochthonous, decreases in this direction below the basin.

3.3. Sediment Infill Geometry From Seismic Interpretation

[17] The main constraint on the basin evolution is given by the sedimentary infill geometry. For the purposes of this work, we adopt the most recent results obtained by *Berástegui et al.* [1998] and *Fernàndez et al.* [1998a], which incorporate field observations and abundant commercial seismic reflection and well log interpretation. According to these studies, the basin is filled by six Miocene seismic-stratigraphic depositional sequences spanning from late Langhian to late Messinian. These Miocene sequences are overlain by Plio-Quaternary sediments, which are prograding westward along the axis of the basin. In contrast, the southern border of the basin is filled by materials corresponding to lateral diapirs of squeezed Triassic evaporites, which in turn developed frontal imbricate wedges. These frontal imbricates involve late Serravallian to late Tortonian sediments (sequences 3 to 5 as given by *Berástegui et al.* [1998]). Sequence 6 (late Tortonian to late Messinian) clearly postdates all the structural features, suggesting that major shortening in the External Betics ended at ~6.3 Ma. The tectonic activity related to normal faulting affecting the basement spans early to middle Serravallian time (sequence 2).

[18] For the sake of simplicity, the six Miocene units described by *Berástegui et al.* [1998] have been grouped into three units (Figure 3): (1) Latest Langhian-Serravallian,

(2) Tortonian, and (3) Messinian. These units correspond to the phases preemplacement, synemplacement, and postemplacement, respectively, of the lateral diapirs and frontal imbricates. The sediment geometry synthesized in Figure 3 includes the offlap of the boundary between Messinian and Plio-Quaternary described by *Sierro et al.* [1996] on the basis of surface discontinuities. The distances displayed are approximate because of the variations along the strike direction. Except for the first Langhian deposits, which are reported as shallow and nearshore, the marine sediments include turbidites. The Plio-Quaternary unit is mostly continental. A striking feature of the geometry of the sedimentary record is the small horizontal distance between the location of the first (Latest Langhian) and the last (Quaternary) deposited units. Figure 3 shows that the four considered units extend to <14 km from the NNW edge of the basin and that the Tortonian unit is shifted toward the active margin of the basin relative to the earlier and later units. A similar long period of depocenter basinward migration at intermediate ages of the basin (~18 Ma) is observed in the Swiss Molasse Basin [*Sinclair et al.*, 1991; *Schlunegger et al.*, 1997].

[19] Accepting that foreland basins are primarily formed by orogenic wedge accretion in their active margin, it is expected that the flexural subsidence propagates toward the foreland, approximately maintaining the basin width (assuming a constant effective elastic thickness [e.g., *Flemings and Jordan*, 1989]. *Sinclair et al*, [1991] explained the basinward migration of depocenters by successive changes in the shape and velocity of the orogenic wedge. Because we lack detailed constraints on the wedge kinematics at the Betic-Guadalquivir system, we assume that thrusting propagates always toward the foreland, as usually observed in the field and shown by analogue models [e.g., *Mulugeta*, 1988] with an arbitrary velocity. Under this assumption, we investigate how the relative basinward location of the Tortonian and Plio-Quaternary units may be related not only to the evolution of the thrusting rate but also to the mechanical response of the lithosphere. The normal faulting affecting the top of the bending plate and its compressive reactivation during the early stages of basin development provide additional constraints for a flexural modeling that accounts for the distribution of stress in the lithosphere.

4. Three-Dimensional Present-Day Load Distribution

[20] Before addressing the relationship between the sediment infill geometry and the lithosphere thermomechanical behavior, we need first to evaluate the origin and relative importance of the different loads responsible for the basin formation. For this purpose, we study the regional isostatic equilibrium using as the main constraint the geometry of the pre-Cenozoic basement of the basin. Flexural calculations have been performed using an elastic thin-plate model with elastic thickness varying from 13 km in the western limit of the basin to 7 km in the east, as constrained by *Van der Beek and Cloetingh* [1992] and the present work. The two-dimensional (2-D) differential equation relating flexural deflection, load distribution, and elastic plate thickness [*Van Wees and Cloetingh*, 1994] is solved by the method of finite differences assuming null derivative and null curvature of the deflection in the boundaries.

[21] As shown by *Van der Beek and Cloetingh* [1992], the flexural formation of the Guadalquivir Basin cannot be explained only by the present-day topographic load, which is a frequent situation in continental settings [e.g., *Brunet*, 1986; *Royden*, 1988; *Buiter et al.*, 1998; *Bott*, 1991]. To estimate the present-day 3-D-load distribution acting in the Betics-Guadalquivir region, we consider that apart from the topographic load, loading is related to crustal and lithospheric thickness variations along time (Figure 4). Because of the lower density of the crust relative to the upper mantle, a thickening of the lower crust would imply buoyant loading. Similarly, a thickening of the lithospheric mantle (denser than the asthenosphere) implies a downward load.

[22] The topographic load is defined as the weight of the column between the present-day topography and the paleotopography at basin initiation minus the weight of the initial water column. Therefore, at the southern margin of the Guadalquivir Basin the topographic load will correspond to the difference between the initial submarine relief and the present relief of the External Betics. At the passive margin of the basin, which corresponds to the Palaeozoic Iberian Massif, we assume an initial plate altitude equal to the mean present topography (350 m), and thus the topographic load is considered to be zero in this area. Prior to the formation of the basin, paleogeographic reconstructions show an inherited Mesozoic passive margin where the relief related to the Palaeogene Internal Betic thrusting was still low and located far from the present basin [*Sanz de Galdeano and Rodŕíguez-Fernández*, 1996]. The shoreline did not change much since the end of Mesozoic until Langhian [*Garčía-Hernández et al.*, 1980; *Sanz de Galdeano and Rodŕíguez-Fernández*, 1996]. Although turbidites are reported in earlier marine deposits [*Sanz de Galdeano and Rodŕíguez-Fernández*, 1996], the first sediments of the present basin (Langhian basal calcarenite) indicate very shallow coastal environments [*Berástegui et al.*, 1998]. On the basis of these studies, we use an initial paleotopography consisting of a shoreline parallel to the present Palaeozoic outcrop, 60 km southward from it, dividing the 350 m altitude in the Iberian Massif from water depths down to 800 m in the present location of the Internal Betics (Figure 4a). Although the paleobathymetry is poorly constrained in the present area of Internal Betics, it will be shown later in this section that its isostatic effect on the model is minor.

[23] The crustal load (related to crustal thickness variation) is calculated as the difference between the present Moho depth and the Moho depth at the beginning of basin evolution, measuring both depths relative to the basin basement. The initial base of the crust is calculated by isostatically compensating (local isostasy) the initial topography (see Figure 4a). Hence the amount of crustal thickness change (CT) excluding the topography component can be

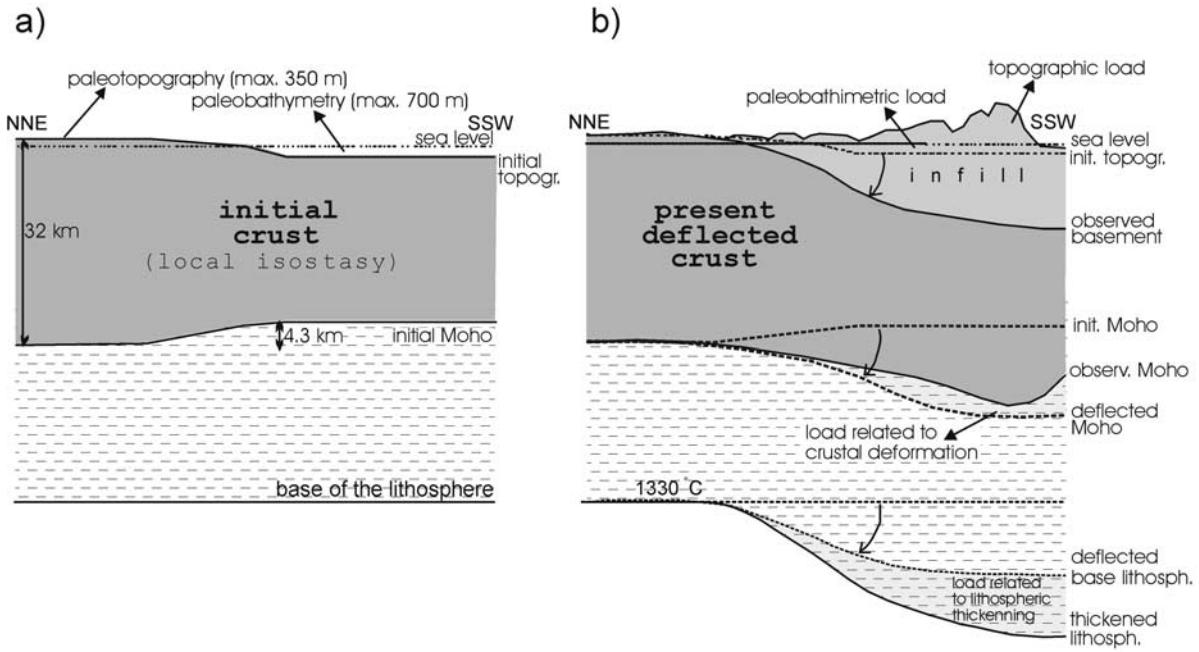

Figure 4. Cartoon showing the different loads accounted for in the planform modeling; not to scale.

written as the difference between the present Moho depth (MD) and the deflected initial Moho, i.e.,

$$\mathrm{CT} = \text{present MD} - \text{initial MD} - \text{observed deflection},$$

assuming that the deflection is positive downward. Finally, the subcrustal load is an unknown that will be deduced from the modeling and then translated in terms of lithospheric thickening/thinning during the formation of the basin.

[24] To determine the present-day load distribution acting on the study region, we must first calculate the distance at which these loads can contribute to the deflection of the Guadalquivir Basin. Figure 5 shows the relative changes induced on the plate deflection W_0 produced in front of a rectangular load of finite length L relative to a load of infinite length. Calculations have been performed assuming an infinite 1D thin elastic plate approach with constant elastic thickness (T_e). Results indicate that for $T_e = 10$ km (a maximum estimate for the Guadalquivir Basin according to *Van der Beek and Cloetingh* [1992]), a load length of 50 km accounts for more than 90% of the deflection produced by an infinite load. Therefore, in terms of flexural analysis the study region is limited to the south by the External Betics, since the loads associated with the Internal Betics and the Alborán Basin are too far from the present-day Guadalquivir Basin to noticeably contribute to its subsidence.

[25] Using the parameter values given in Table 1. and bearing in mind the above considerations, we first calculate the deflection produced by the loads related to topography and crustal deformation. Figure 6a shows the basement depth (i.e., deflection plus paleotopography) resulting from applying the mass difference between the paleotopography and the present-day topography (topographic load). Paleobathymetry is a relevant factor increasing the topographic load and all materials above the initial paleosurface have been considered as topographic load. In fact, an important part of the deflection shown in Figure 6a is related to the initial paleobathymetry rather than to the present-day relief above sea level. However, the predicted basement depth is insufficient to explain the observations in Figure 2a.

[26] The subsidence obtained when including the load related to crustal thickness changes is shown in Figure 6b. In this case, the predicted basement depth is closer to that observed, but still a positive (downward) additional load is required to reproduce the deflection of the Iberian plate. This additional load is calculated by using a forward modeling technique to fit the observed basement depth shown in Figure 2a. The resulting load distribution is shown in Figure 7 in terms of lithospheric thickening using a mean-density contrast between the lithospheric mantle and the asthenosphere of 50 kg m^{-3}. According to these results, the thickening of the lithospheric mantle increases to $\sim$30 km beneath the External Betics showing small variations along strike and vanishing progressively toward the northern limit of the basin. The amount of thickness variation is subjected to the uncertainty of the initial topography, which in turn constrains the initial crustal configuration. Overestimating the paleobathymetry at the present basin domain in 200 m (i.e., considering that the Langhian coastal basal calcarenites were deposited 200 m deep) produces a 25% reduction of the predicted lithospheric thickening. Although the uncertainty in the paleobathymetry farther to the south (present Betics) is higher, its isostatic effect is reduced because of the larger distance to the present basin location. Thus, although keeping in mind this uncertainty in the

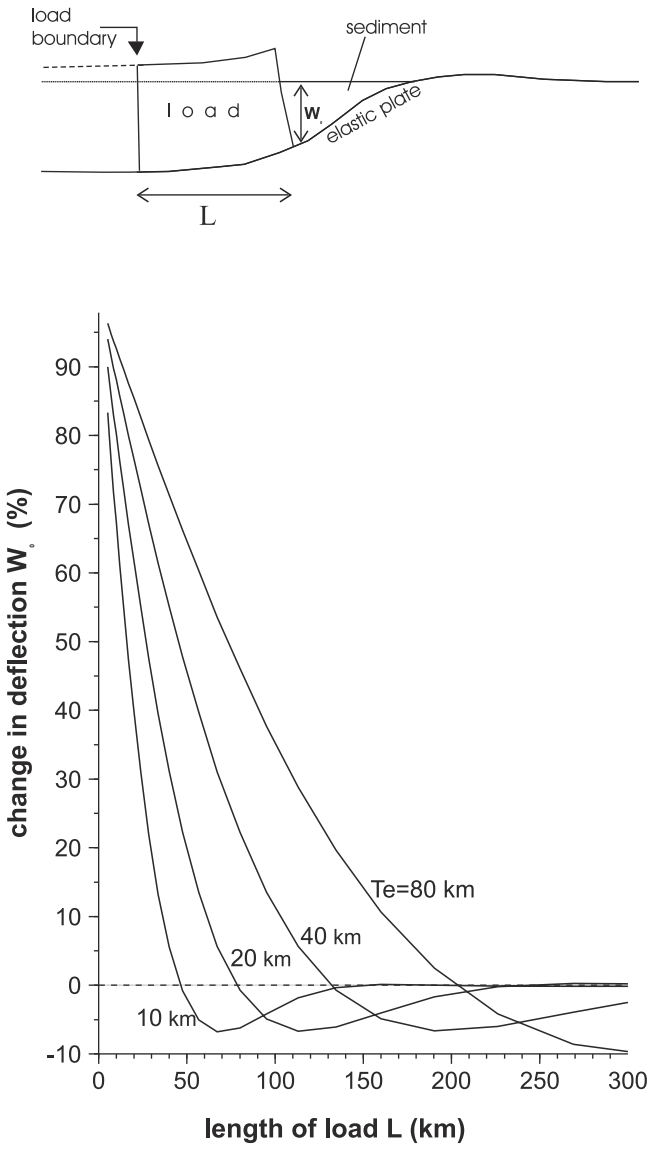

Figure 5. Parameterization showing the change induced on the maximum deflection W_0 at the basin when varying the length of the load L included in the model. The change in deflection (%) is relative to the deflection produced by an infinite load ($L = \infty$). For low values of elastic thickness T_e, the effect of the distant part of the load is negligible.

lithospheric thickening distribution, the effect of paleobathymetry [*Van der Beek and Cloetingh*, 1992] reveals insufficient to explain the hidden load associated with the Guadalquivir Basin.

[27] Thickening of the lithospheric mantle beneath the Guadalquivir Basin region is also supported by gravity and geoid data. The coincidence of Bouguer and geoid minima in the Guadalquivir region [*Fernàndez et al.*, 1998a] is a rather unusual feature in crustal thickening areas. An interpretation of this feature in terms of crustal and lithospheric geometry is undertaken below based on 2-D gravity field calculations based on the algorithms by *Talwani et al.* [1959] and *Chapman* [1979]. Figures 8a and 8b show the calculated gravity and geoid anomalies for three lithospheric geometries under isostatic compensation generating a topographic elevation of 800 m (representing the mean value of the Betics relative to the Iberian foreland). The results show that a simple crustal or homogeneous crust/mantle thickening (cases 1 and 2 in Figure 8a) do not predict a geoid low. Instead, to reproduce the geoid and Bouguer anomalies of similar magnitude to that observed in the Betic-Guadalquivir system (Figure 8c), it is necessary that the lithospheric mantle thickens twice as much as the crust (case 3 in Figures 8a and 8b). In case 3, the crust and the mantle thickening have been mutually shifted 50 km to simulate the thickening geometry derived in this work.

5. Modeling the Basin Evolution

[28] The present-day load distribution acting on the Guadalquivir Basin region shows that despite the topography (and hence the topographic load) having important variations along strike (higher in the Central Betics than in the Western Betics), the total load has an acceptable 2-D (cross section) symmetry. This is reflected in the small lateral variations along strike of the flexural subsidence (Figure 2a) and suggests that the evolution of the basin can be addressed by modeling a representative cross section (located in Figure 1). The objective of this modeling is to quantitatively link the basin infill evolution with the lithosphere rheology using a simple kinematic model of the emplacement of the External Betics and the subcrustal loads determined in the previous section. Although the model is mainly constrained by the present-day basement depth and the geometry and timing of the sedimentary basin infill, additional observations such as the reactivation of basement faults and the uplift of Sierra Morena will be also considered. In order to fit those constraints, forward modeling is performed varying the parameters controlling the lithospheric, tectonic, and erosion/sedimentation processes.

[29] The cross-sectional models below are based on a finite difference code that links the load associated with the emplacement of thrust sheets with the surface mass transport and the mechanical behavior of the flexed lithosphere [*Garcia-Castellanos et al.*, 1997; *Garcia-Castellanos*, 1998]. Thrust sheet kinematics are calculated by vertical shear, i.e., preserving the vertical thickness of every thrust-

Table 1. Parameters Used for the Elastic 2-D (Planform) Model of Present-Day Load Distribution

	Value
T_e	7–13 km
Density of topography	2700 kg m^{-3}
Density of water	1013 kg m^{-3}
Density of infill	2700 kg m^{-3}
Density of crust	2800 kg m^{-3}
Density of mantle	3300 kg m^{-3}
Density of asthenosphere	3250 kg m^{-3}
Gridding	6 × 6 km
Maximum initial altitude	350 m

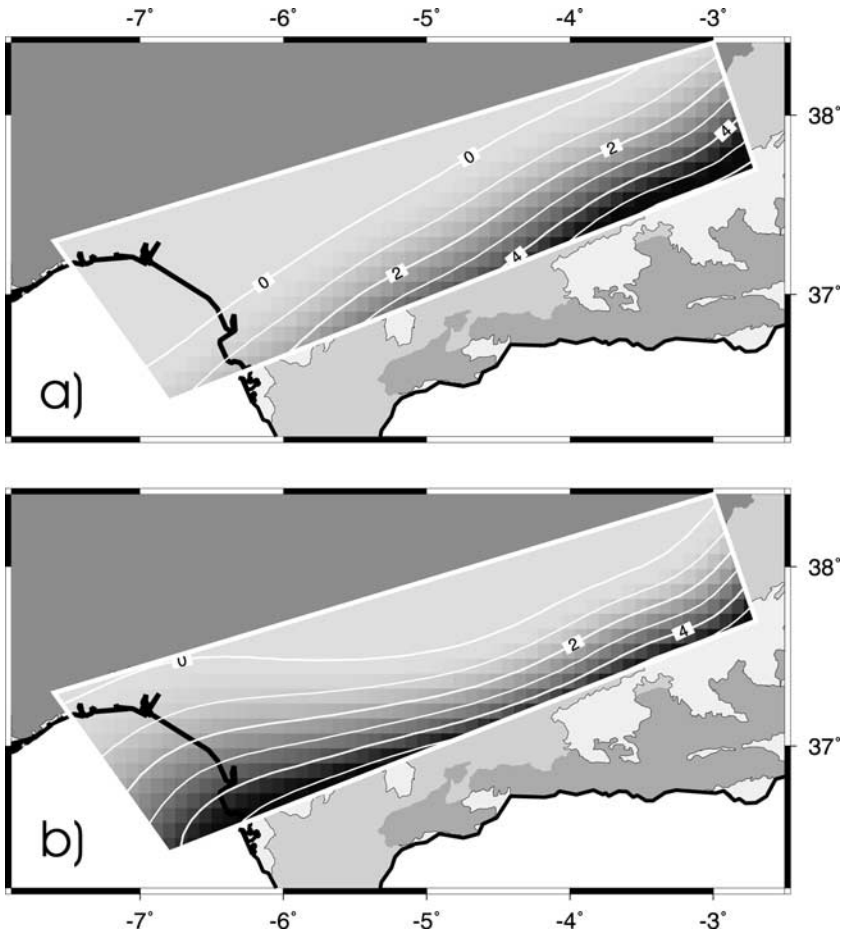

Figure 6. Predicted basement depth (kilometers) relative to the present sea level. (a) Deflection due to the topographic/bathymetric load. (b) Same as Figure 6a but adding the effect of crustal thickness variations.

ing unit during their movement and assuming that thrusting propagates toward the foreland. The thickness of the thrusting units (5 km) is constrained by the geological cross sections of *Berástegui et al.* [1998] and *Fernàndez et al.* [1998a], whereas the shortening velocity has been arbitrarily defined to fit the final basin volume. The timing of shortening applied (4 km Ma^{-1} before 10.5 Ma; 2.5 km Ma^{-1} between 10.5 and 6.5 Ma and 0 km Ma^{-1} after 6.5 Ma) is

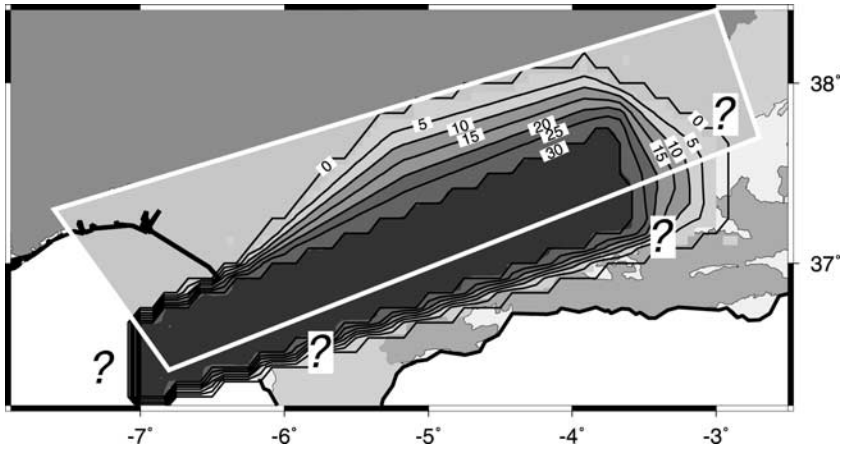

Figure 7. Resulting sublithospheric load depicted in terms of lithospheric mantle thickening (kilometers) assuming a density contrast relative to the asthenosphere of 50 kg m^{-3}.

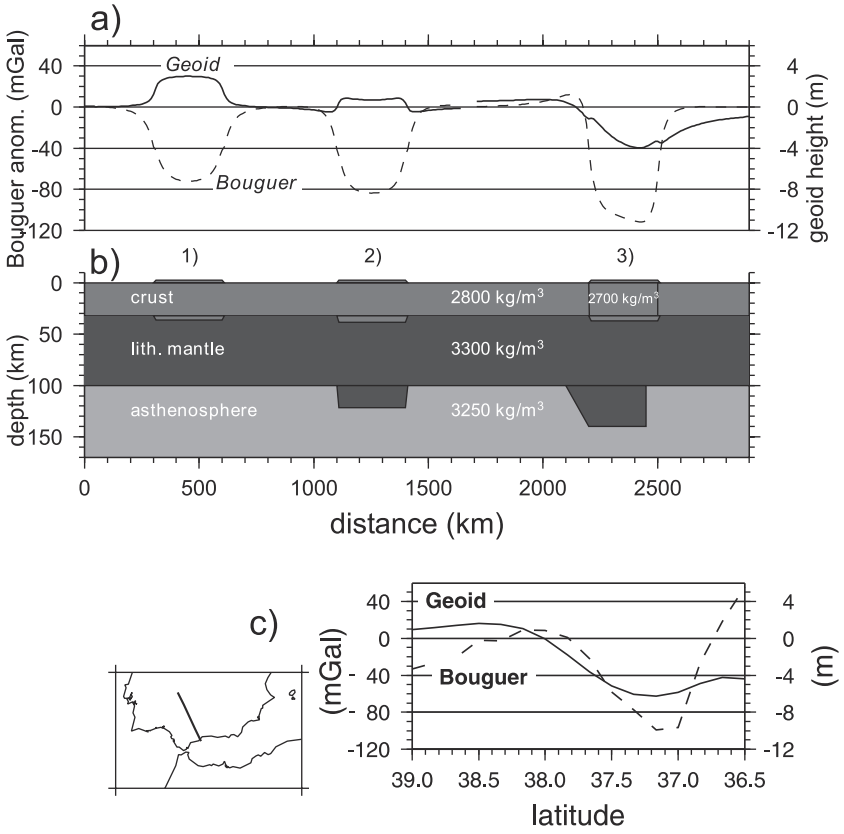

Figure 8. (a) Bouguer gravity and geoid anomalies produced by (b) three different amounts of crust and lithospheric thickening. Topography in Figure 8b is exaggerated by a factor 3 in respect to the other bodies. Cases 1 and 2 correspond to crustal and lithospheric uniform thickening, respectively. Case 3 corresponds to a lithospheric thickening where mantle thickens double than crust. (c) Profile of the observed gravity (Bouguer) and geoid anomalies.

constrained with the end of compressional deformation of the frontal sediment imbricates observed in seismic profiles [*Berástegui et al.*, 1998]. The total amount of shortening in the last 18 Myr is 40 km, which implies a total volume of thrust-generated relief of 200 km^2 (cubic kilometer volume per kilometer length along the strike). It must be noted that the initial time of the model does not correspond to the first shortening episodes recorded in the External Betics but to those that produced basement deflection in the region occupied by the present-day Guadalquivir Basin.

[30] The sedimentary record of the Guadalquivir Basin (see Figure 3 and *Berástegui et al.* [1998]) shows that the southern margin of the basin consists of a lateral diapir of Triassic evaporites and a frontal north verging imbricate wedge involving Tortonian sediments. Our modeling does not intend to reproduce either the emplacement of the Triassic evaporites or the deformation of the frontal Miocene imbricates. Nevertheless, for loading purposes we have considered that Triassic evaporites contribute to basement deflection, whereas the Miocene imbricates form part of the sedimentary infill disregarding its internal structure. In consequence, the frontal thrusts resulting from our models (e.g., Figure 9) must be geometrically interpreted as the frontal part of the lateral Triassic diapirs. The sedimentation rate was higher during the Messinian, when a similar sediment thickness to the other units was deposited in a shorter time [*Berástegui et al.*, 1998]. This leads us to incorporate to the model the subcrustal loads derived in the previous section at the time t = 6 Ma (as an instantaneous load), although this choice depends on the approaches used in the sedimentation model.

[31] The sedimentation rate varies laterally according to the available space below sea level, and it is limited with a maximum value (Tables 2 and 3). The subaerial erosion rate is proportional to altitude above sea level except for the Plio-Quaternary period, during which the level dividing erosion and sedimentation has been raised 100 m above sea level to reproduce the complete infill of the basin with continental sediments. Sedimentation and erosion constants were modified to fit the observed sedimentary unit thickness as displayed in Figure 3 and the present-day topography and basement depth. No mass conservation is considered between erosion and sedimentation, since transport in the strike direction has been dominant during the basin history. At each time step, a new increment in flexural deflection is calculated from the load redistribution produced by thrusting and erosion/sedimentation. The model numerical domain 400 km long.

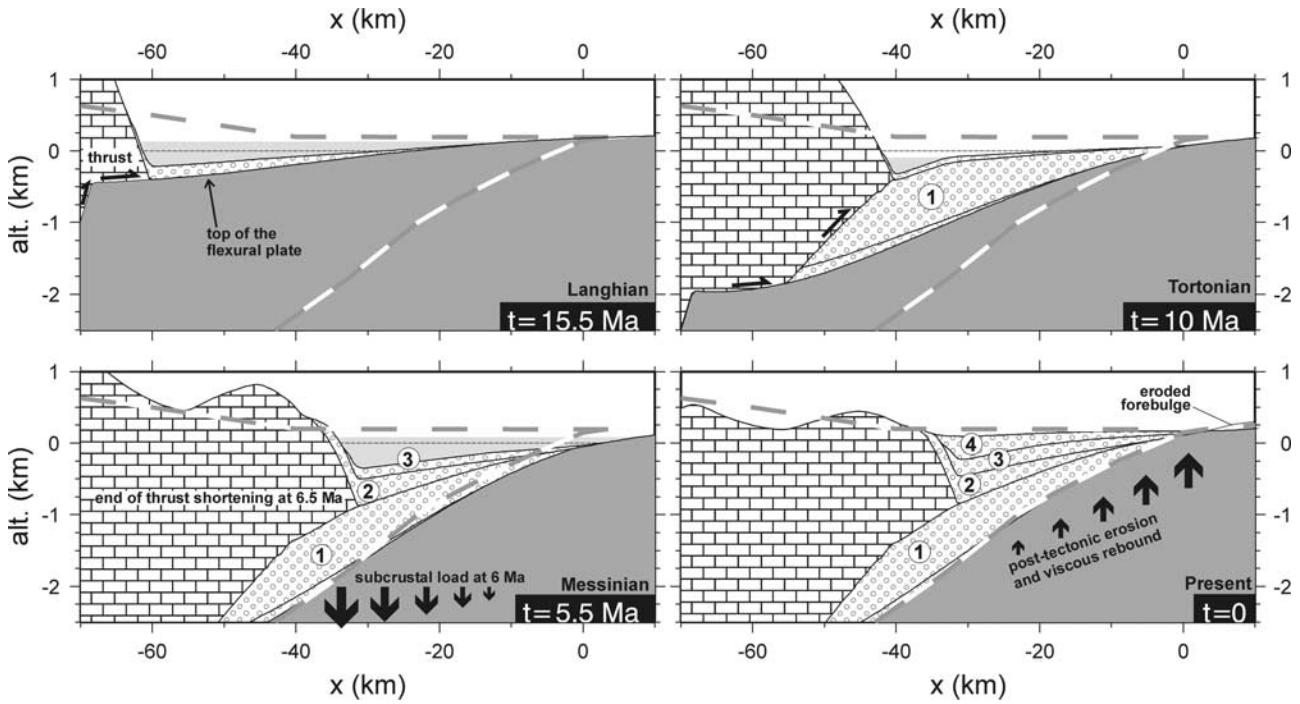

Figure 9. Basin geometry resulting from the viscoelastic model at different time steps. Vertical coordinates are relative to the present-day sea level. Dashed thick lines show the present-day observed mean altitude and basement depth. The light shading shows the water body. Sedimentary units are as follows: 1, Latest Langhian-Serravallian; 2, Tortonian; 3, Messinian; 4, Plio-Quaternary.

[32] First tentative models have shown that it is not possible to reproduce the Tortonian basinward shift of the position of the onlap (Figure 3) by using a pure-elastic plate model and a thrusting propagation toward the foreland, since this predicts a continuous onlap of sequences as found also by *Flemings and Jordan* [1989]. On the other hand, incorporation of eustatic curves [*Haq et al.*, 1987] to these models showed that sea level variations are insufficient to explain the strong Tortonian basinward shift of the pinch-out observed in the Guadalquivir Basin. Because of the important basement dip reached at Tortonian, the migration of the pinch-out in this period would require an unreasonable eustatic sea level change of 300–500 m. Therefore we investigate two complementary mechanisms that may cooperate with eustasy to explain the shift of the pinch-out during the Tortonian: viscous relaxation of the lithospheric stresses, and elastic-plastic yielding within the lithosphere.

5.1. Viscoelastic Model

[33] According to the viscoelastic model of lithospheric flexure [e.g., *Nadai*, 1963; *Beaumont*, 1981], after responding elastically to a load, the lithosphere presents a time-dependent deflection related to the viscous relaxation of the stress within the plate. This viscous relaxation reduces the wavelength of the deflection pattern through time, producing a basin narrowing similar to that caused by a reduction in elastic thickness. The velocity of this viscous deformation is controlled by the relaxation time parameter τ, related to the viscosity of the plate. We solve via the finite difference method the equation governing a viscoelastic plate. This equation relates the deflection profile to the external acting loads and plate parameters (elastic thickness and relaxation time), and is based on the standard thin-plate approach [e.g., *Beaumont*, 1981]. At each time step of the numerical model a new deflection increment is calculated and added in terms of subsidence/uplift to the basin profile. Further details on the applied technique are given by *Garcia-Castellanos et al.* [1997].

Table 2. Parameters Used for the Viscoelastic 1-D (Cross Section) Model

	Value
T_e	15 km
Relaxation time τ	1.2 Myr
Initial time	18 Ma
Final time	0 Ma
Shortening velocity before t = 10.5 Ma	4 km Myr^{-1}
Shortening velocity from t = 10.5 to t = 6.5 Ma	2.5 km Myr^{-1}
Sediment density	2300 kg m^{-3}
Horizontal tectonic compressional force F_x	0 N m^{-1}
Basement and crust density	2700 kg m^{-3}
Erosion rate K_{EC}	0.09 m m^{-1} Myr^{-1}
Maximum sedimentation rate K_{SM}	160 m Myr^{-1}
Gridding dx	0.5 km
Maximum initial altitude	350 m

Table 3. Parameters Used for the Elastic-Plastic 2-D (Cross Section) Model[a]

	Value
Thermal lithosphere thickness	93 km
Mechanical lithosphere thickness	53 km
Crustal thickness	32 km
Upper crust thickness	21 km
Initial time	22 Ma
Final time	0 Ma
Shortening velocity before t = 10.5 Ma	4 km Myr^{-1}
Shortening velocity from t = 10.5 to t = 6.5 Ma	2.5 km Myr^{-1}
Sediment density	2300 kg m^{-3}
Basement and crust density	2700 kg m^{-3}
Erosion rate K_{EC}	0.12 m m^{-1} Myr^{-1}
Maximum sedimentation rate K_{SM}	200 m Myr^{-1}
Gridding dx, dz	0.5, 0.6 km
Horizontal tectonic compressional force F_x	-0.3 TN m^{-1}

[a] Other parameter values are as in Table 2.

[34] Figure 9 shows the evolution of the best fitting viscoelastic model of the Guadalquivir Basin using a viscoelastic plate. The parameter values required during the forward modeling are summarized in Table 2. The last stage in Figure 9 (t = 0) shows that the viscoelastic approach satisfactorily reproduces the present-day basement geometry, the sedimentary infill geometry, and the mean topography. In agreement with the observed sedimentary record (Figure 3), the Tortonian and Plio-Quaternary depocenters migrate basinward relative to the Latest Langhian-Serravallian and Messinian units, respectively. The basin geometry is here a result of the competition (at each time step of the model) between the instantaneous elastic response to thrusting (that shifts the basin depocenter toward the foreland) and the speed of viscous relaxation (that narrows the basin and uplifts it distal margin). During the syntectonic phase, thrust loading and its associated elastic flexural response are the leading processes, prevailing over the erosion unloading and the viscous relaxation and generating a foreland basin together with the subcrustal load acting at 6 Ma. In the posttectonic period (after 6 Ma), only the viscous relaxation takes place, reducing the basin width and uplifting its sediment infill (particularly in the distal part). The incorporation of the subcrustal load derived from the planform modeling produces an increase in bathymetry in the basin and a reduction of the topography in the orogen. The calculated maximum bathymetry is 350 m, coinciding with the emplacement of the subcrustal load (Figure 9), but it depends on the sedimentation rate, which is in turn poorly constrained. Finally, the erosion and sedimentation processes lead to the present low topography and overfilled basin.

[35] The flexural forebulge at the final stage is centered between x = 20 km and x = 45 km. The maximum rebound there is 174 m, though most of this relief has been eroded (dotted line in Figure 9). The predicted location of the forebulge coincides with Sierra Morena, the mountain range bounding the basin to the north and acting as water divide between the Guadalquivir drainage basin and the Iberian Massif. The predicted amount of uplift is smaller but comparable to the mean height of this range relative to the Iberian Massif (~300 m), suggesting that forebulge uplift could be a first-order process contributing to the formation of Sierra Morena. Incorporation of horizontal compression throughout the evolution (reflecting the overall convergence between Iberia and Africa) and minor parameter changes with respect to the model shown in Figure 9 enhances the forebulge uplift by buckling the lithosphere, while preserving a good fit of the basin geometry. However, rather than finding the horizontal force by fitting a poorly constrained forebulge uplift, the calculation of this force is addressed in section 5.2 by means of an elastic-plastic model that attempts to account for the stress evolution in the plate.

5.2. Elastic-Plastic Model

[36] A second lithosphere mechanical behavior that can explain the characteristics of the sedimentary infill geometry of the Guadalquivir Basin is plastic yielding. According to this plate model, the lithosphere behaves elastically below a certain yield stress that varies in depth. When this yield stress is reached, anelastic deformation takes place and the apparent rigidity of the plate is reduced. *Waschbusch and Royden* [1992] demonstrated that the elastic-plastic stratification of the lithosphere could induce a nonlinear flexural response that generates sedimentary unconformities. Following these authors, we use similar approaches to model the evolution of the basin geometry. We refer to *Garcia-Castellanos et al.* [1997] and *Garcia-Castellanos* [1998] for a detailed description of the elastic-plastic multilayered plate model used in this work. A significant improvement has been made to their model: Instead of calculating the stress distribution in the elastic-plastic plate as a function of the plate curvature at every time step, here we add stress increments to the cumulated stress distribution (similar to *Waschbusch and Royden* [1992]).

[37] The main differences between the viscoelastic and the elastic-plastic models (compare Tables 2 and 3) are (1) the rheological behavior of the lithosphere; (2) in order to reach the earlier stages of basin evolution with a quasi steady state stress accumulation in the plate, the modeling initiates at t = 22 Ma instead of t = 18 Ma, and an additional thrust unit is active during this new period; and (3) a constant horizontal tectonic force of $F_x = -0.3$ TN m^{-1} causing an overall compressive regime is incorporated throughout the model evolution to increase the tilting of

Table 4. Parameters Used to Calculate the Geotherm and the Yield Stress Envelope of the South Iberian Lithosphere (Figure 10)[a]

	Thickness, km	k, W m^{-1} K^{-1}	H_{RP}, μW m^{-3}	$\dot{\varepsilon}_o$, M Pa^{-n}s^{-1}	Q*, KJ mol^{-1}
Upper crust	21	2.5	1.4	2.5×10^{-8}	140
Lower crust	11	2.1	0.2	3.2×10^{-3}	250
Lithospheric mantle	93[b]	3.1	0	10^3	523

[a] Rheological parameters (n, $\dot{\varepsilon}_o$ and Q*) taken from *Lynch and Morgan* [1987].
[b] Calculated depth of the 1330°C isotherm.

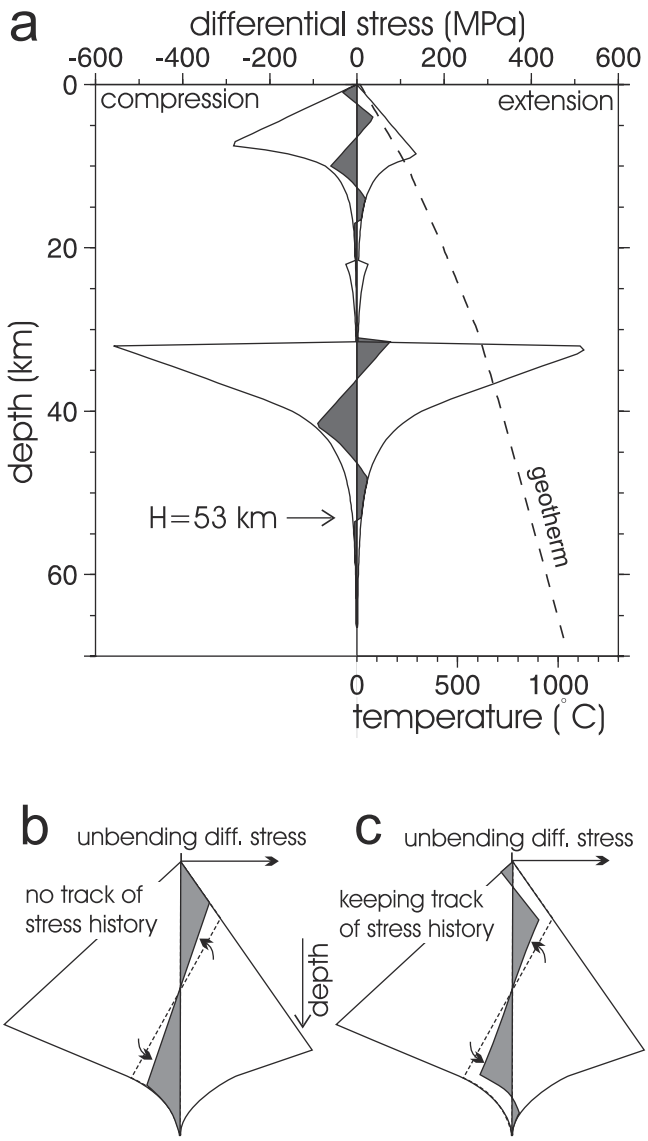

Figure 10. (a) Geotherm (dashed line) and stress envelope calculated for the elastic-plastic plate model. The strength is nearly zero in the lower crust, and the thermal lithosphere is relatively thin (93 km). The mechanical thickness of the lithosphere (depth to which strength is higher than 10 MPa) is 53 km. The shaded area shows the stresses obtained at $x = -34$ km and for $t = 0$ Ma. The recent stress inversion (from extensive to compressive) can be observed in the top of the plate. (b and c) Cartoons showing schematically the way the bending stresses (dashed lines) are redistributed during unbending (shaded). When stress history is accounted for (Figure 10c), unbending produces immediate inversion of the stress at the top of the plate, whereas if stress is calculated simply as a function of plate curvature (Figure 10b), unbending does not necessarily imply stress inversion.

the basement without further weakening of the thermal structure of the lithosphere. This force reflects qualitatively the overall collisional regime between Iberia and Africa during the formation of the basin and the present NNW-SSE compressional regime in Iberia.

[38] The mechanical response of an elastic-plastic plate is determined by means of the yield stress envelope (YSE) concept [e.g., *Lynch and Morgan*, 1987]. We have constructed an YSE for the Iberian lithospheric plate based on the measured surface heat flow [*Fernàndez et al.*, 1998b] and using standard rheological parameters (Table 4). To calculate the geotherm shown in Figure 10a we use three layers of constant thermal conductivity k and radiogenic heat production H_{RP}, with a surface heat flow of 66 mW m^{-2} [*Marzán et al.*, 1996; *Fernàndez et al.*, 1998b]. The resulting base of the thermal lithosphere (1330°C isotherm) is located at 93 km depth. To derive the yield stress at each depth from the temperature profile, we use a deformation rate of $\dot{\varepsilon} = 10^{-16}$ s^{-1}. The vertical discretization interval of the plate is $dz = 0.6$ km. The resulting YSE (Figure 10a) shows a mechanical thickness (depth above which strength >10 MPa) of 53 km and a very low strength at the base of the crust, indicating a probable mechanical decoupling between crust and mantle. The integrated lithospheric strength is 5.4×10^{12} N m^{-1} (compression) and 4.6×10^{12} N m^{-1} (extension). The equivalent elastic thickness of this elastic-plastic plate is not assumed a priori, but it is a result of the YSE and the history of the deflection profile curvature. The predicted values of T_e at the last stage vary laterally from 25.1 km in the areas distant from the basin down to 6.7 km below the basin, where the deflection has a higher curvature.

[39] A major factor controlling the final stress distribution is the irreversibility of plastic deformation and the cumulative stress history [*Mueller et al.*, 1996a, 1996b]. If this process is dismissed (i.e., stress distribution is calculated only as a function of the present curvature; Figure 10b), then the inversion of stresses at the top of the plate is predicted at an inflexion point of the deflection profile, where curvature changes in sign. Instead, in our modeling the inversion occurs over a maximum curvature point (Figure 10c). The reader is referred to the work by *Mueller et al.* [1996a, 1996b] for further details on this subject.

[40] The resulting basin geometry (Figure 11) is in good agreement with the observed sediment units (Figure 3) and the basinward migration of the onlap during Tortonian is satisfactorily reproduced. This geometry is here the result of the competition between the thrusting toward the foreland and the reduction in equivalent elastic thickness related to the increase in plate curvature (which induces a basin narrowing similar to the viscous relaxation in the previous model), explaining the Tortonian depocenter migration toward the wedge. The Messinian progradation of the onlap is due to the subcrustal loading at 6 Ma. The main parameter controlling the final basin geometry is the surface heat flow, which determines the geotherm and the strength distribution. The best fitting value (66 mW m^{-2}) is within the range of observations derived from oil and water well measurements [*Fernàndez et al.*, 1998b].

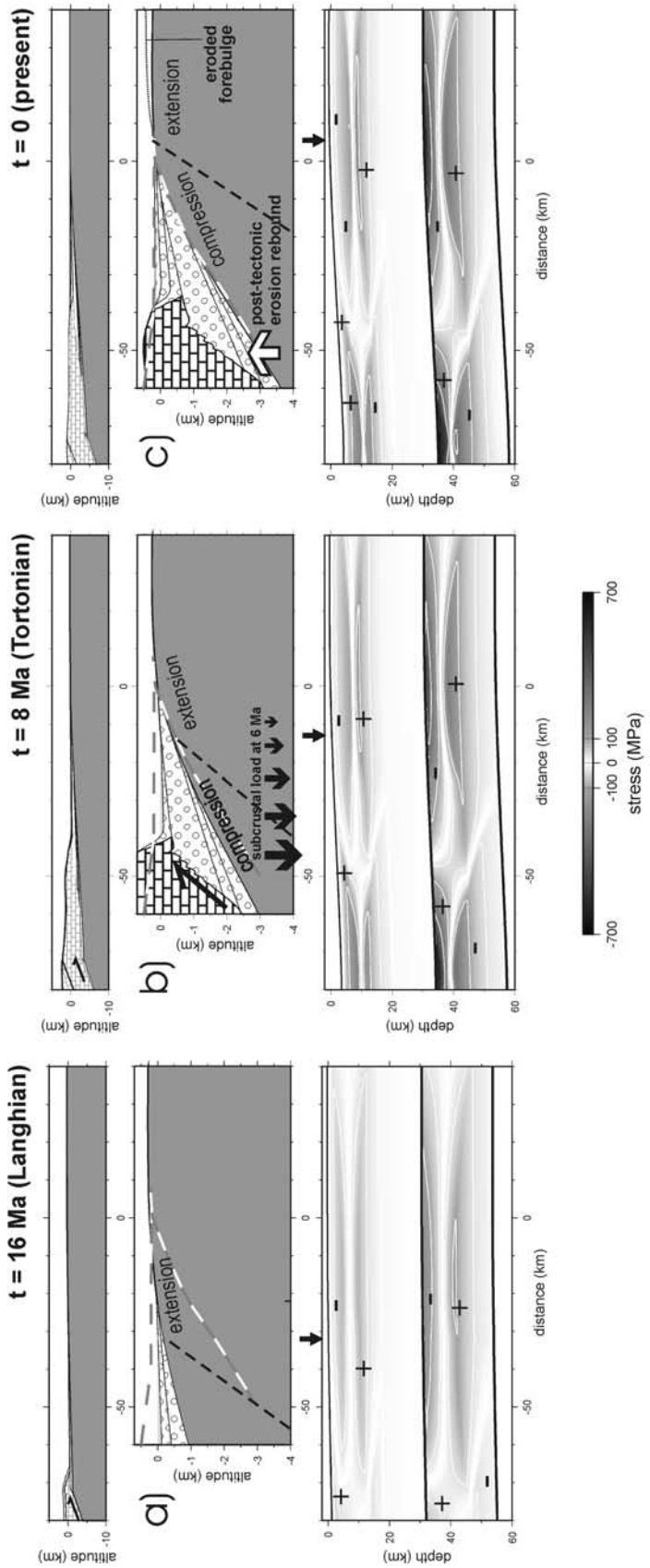

Figure 11. (a–c) Basin geometry obtained from the elastic-plastic model at 16, 8, and 0 Ma. Top plots show true-scale cross section; middle plots show enlargement of the basin (vertical exaggeration $\times 10$). Dashed lines separate regions of extensional and compressional yielding (stress is yield stress); Bottom plots show stress distribution within the plate. Arrow marks the point on the top of the plate where the inversion of the stress is occurring (extensional to right and compressional to left). Dashed lines in middle plots correspond to the present basement and topography (both averaged along strike). Sedimentary horizons correspond to $t = 18$, 15.5, 10.5, 6.5, 5, and 0 Ma (compare with Figure 3).

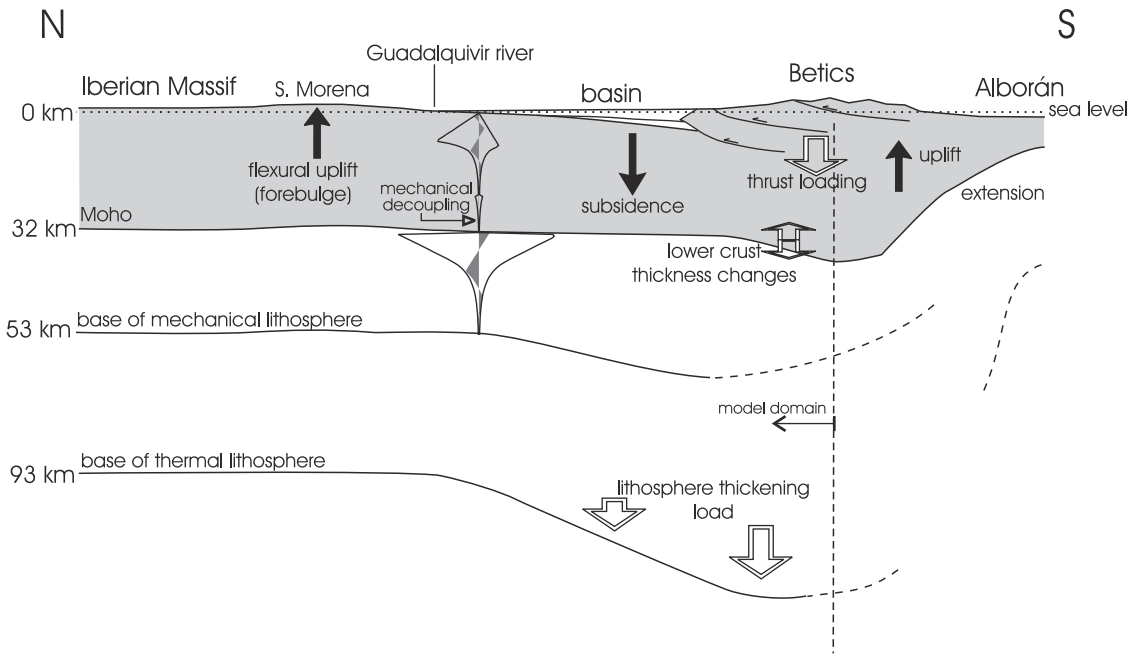

Figure 12. Cartoon showing the processes related to the formation of the Guadalquivir Basin. The load related to crustal and lithospheric thickening produces subsidence in the basin and uplift in Sierra Morena. Rheological layering and mantle-crust decoupling permit to explain the history of sedimentation and stress. Isostatic forces (open arrows) and associated vertical movements (solid arrows) are indicated.

[41] The other best fitting parameter values (Table 3) do not differ substantially from those found in the viscoelastic model. The most significant result from the elastic-plastic model is that it predicts the change in the lithospheric stress regime recorded by near-vertical faults affecting the basement [*Berástegui et al.*, 1998]. Figure 11 shows the calculated stress distribution at different time steps showing that the top of the present-day basin (from $x = -40$ to $x = 0$ km) changes from an extensional regime at $t = -15.5$ Ma to a compressional regime at present. Thus the elastic-plastic model provides a self-consistent explanation for the reactivation of normal faults as inverse faults in the basement as based on the thermomechanical structure of the South Iberian lithosphere.

6. Discussion

[42] The evolution of a foreland basin is approached in this work by integrating orogenic wedge formation, lithospheric flexural stress distribution, erosion/sedimentation, and deep crust and mantle deformation. The application of this technique to recent data compilations that constrain the evolution of the Guadalquivir Basin gives a quantitative insight of the processes involved and provides an interesting perspective of the evolution of foreland basins.

6.1. Hidden Loads

[43] The analysis of the 3-D present-day load distribution in the Guadalquivir Basin shows that the subsidence experienced in the basin can be explained by the stacking of the External Betics on the foreland in combination with the loading effect related to deeper processes. The magnitude of this deeper load is slightly lower and shifted to the north than the extra load deduced by *Van der Beek and Cloetingh* [1992], partially because we incorporate the effect of the initial bathymetry on the topographic load.

[44] Additional (or hidden) downward loads required in flexural studies are mostly related in the literature to subduction slab pull [*Royden*, 1993] and/or to dynamic topography [*Burgess and Moresi*, 1999], but the lack of evidence for these processes in South Iberia demands alternative sources. Our interpretation in terms of thickening of the lithosphere (Figure 12) under the Betics is compatible with the observed gravity and geoid lows in the Guadalquivir Basin (Figure 8) and is supported by a recent 3-D gravity and heat flow modeling [*Torne et al.*, 2000] revealing that the base of the lithosphere beneath the Betics lies at 140 km depth, in contrast to the 110 km proposed for the stable Iberian Peninsula. A similar deepening of the lithosphere toward the south is inferred by *Calvert et al.* [2000] and *Seber et al.* [1996] on the basis of tomographic and earthquake hypocenter studies. A major question arises in the interpretation of this mantle thickening. The results of *Calvert et al.* [2000] support the idea that the south Iberian lithospheric mantle is delaminating (“peeling”) from the crust below the Alborán-Betics region and sinking into the asthenosphere. This process would have initiated at late Oligocene-early Miocene times affecting, essentially, the extending Alborán Domain. The progressive peeling back of the lithospheric mantle (coeval with the convergence between the African and the Iberian plates) displaced the delaminated lithosphere toward the NW. The pull effect of

this ''lithospheric root'' would have influenced the Guadalquivir Basin since 6 Ma, explaining the lithospheric thickening found in our study.

[45] This interpretation suggests also that the commonly invoked additional or hidden loads may be partially related to lithospheric thickening occurring independently at crustal and mantle levels during plate collision. The sign and magnitude of these loads depend on the initial lithospheric geometry and on the resulting ratio of crust/mantle deformation whatever the deformation mechanism is.

6.2. Mechanical Behavior of the Lithosphere

[46] Low values of equivalent elastic thickness as those found for the Guadalquivir Basin are frequent in noncratonic continental settings [*Watts*, 1992; *Stewart and Watts*, 1997] and their origin is not fully understood. Four mechanisms have been explicitly accounted for in this work to explain the low rigidity of the lithosphere: (1) viscous relaxation of stresses during flexure; (2) plastic yielding in the lithosphere during its bending; (3) mechanical decoupling between crust and mantle; and (4) presence of a compressional tectonic force during bending.

[47] Present-day deflection profiles can be commonly reproduced by simple elastic plate models. In foreland basins, the unique role of the sedimentary infill as a recorder of the flexural evolution offers the opportunity to further understand the heterogeneous mechanical behavior of the continental lithosphere, arising the necessity for more sophisticated rheological models. In the Guadalquivir-Betic system, an elastic flexural model loaded by thrust deformation propagating toward the foreland (as normal during growth of accretionary wedges) [e.g., *Davis et al.*, 1983; *Mulugeta*, 1988] cannot explain the important basinward shift of the onlap during the Tortonian (Figure 3). Therefore we investigate the role of nonelastic behavior of the lithosphere during basin formation.

[48] The effect of a nonelastic component in the bending of the lithosphere during foreland basin evolution has been recognized separately by workers such as *Beaumont* [1981] (effect of viscoelasticity) or *Waschbusch and Royden* [1992] (effect of elastoplasticity). In the present work, both viscoelasticity and elastoplasticity have been shown to be capable of explaining the sedimentary record of the Guadalquivir Basin, but none of these rheological properties can be dismissed because each can explain different secondary observations (forebulge uplift and evolution of basin basement faults, respectively). Both rheologies should be viewed therefore as complementary and pointing to the necessity of accounting for a fully elasto-visco-plastic rheology in future basin analyses.

[49] The application of the elastoplastic multilayered approach to the Guadalquivir Basin has allowed us to explain the evolution of the extensional faults in the basement and to directly link the basin sedimentation history with the lithospheric structure derived from heat flow and deep seismics. This shows that modeling the large-scale geometry of foreland basin sedimentary units can help to understand not only the tectonic evolution of orogenic wedges, but also the complexity of the mechanical behavior of the lithosphere.

6.3. Forebulge Uplift

[50] Forebulge uplift, though widely referred in the literature of foreland basins, has been mostly reported through its effect on the sedimentary record (e.g., the Molasse Basin) [*Crampton and Allen*, 1995], and therefore it is constrained typically by seismic imaging rather than by direct on-site observations. The viscoelastic flexural model used in the present work suggests that the present relief of Sierra Morena corresponds to the subaerial flexural forebulge of the Guadalquivir Basin. This interpretation is supported by independent evidence such as the increase of erosion rates in Sierra Morena during Neogene deduced from fission track analysis [*Stapel*, 1999, Figures 6–11 and 6–12], the rise of the Moho below Sierra Morena [*González et al.*, 1998], and the stress regime derived from fault population and seismicity [*Herraiz et al.*, 1996]. Although the uplift predicted by the viscoelastic model is smaller than the mean elevation of the Sierra Morena relative to the Iberian Massif, the overall NW-SE compressional stress regime in Iberia may enhance this uplift by lithospheric folding [*Cloetingh et al.*, 1999, 2002]. Preliminary tests incorporating a compressional tectonic force into the viscoelastic model resulted in increased forebulge uplift closer to the observed topography while preserving a good fit of the basin infill geometry, though the force required was about double than that constrained through the elastic-plastic model. The recognition of the Sierra Morena as a forebulge-plus-folding feature may be further constrained in the future by means of river incision studies of the northern tributaries of the Guadalquivir River and by isotope-based denudation studies.

6.4. Kinematics of the Betics and Surface Mass Redistribution

[51] To quantitatively reproduce the evolution of the Guadalquivir Basin by fitting the geometry of the sediments, we require the NNW shortening rate in the frontal orogenic wedge to decrease during the Tortonian (10.5–6.5 Ma) and eventually stop at the very late Tortonian, in agreement with the deformation observed in the frontal sediment slices [*Berástegui et al.*, 1998; *Fernàndez et al.*, 1998a]. We demonstrate that because of the weakness of the South Iberia lithosphere, the evolution of the Guadalquivir Basin was only sensitive to loads applied at distances <50 km from the thrust front. This restriction has two important consequences: (1) The kinematics of the Internal Betics and the Alborán Basin have no isostatic effect on the sedimentary record of the Guadalquivir Basin and (2) the kinematics of the External Betics prior to the middle Miocene is not recorded either by the sedimentary infill or by the basement geometry, since earlier thrusting occurred too far away to exert any significant influence on the present basin location.

[52] Because of the 2-D (cross section) character of the numerical experiments incorporating sedimentation, the

surface mass transport cannot be reproduced with a mass-conservative model. Therefore the resulting erosion/sedimentation rates must be interpreted separately as values necessary to fit the present-day topography of the External Betics (erosion) and the geometry of the sedimentary infill (sedimentation). The difference between the total eroded and deposited mass is attributed to additional sediment supply from two sources which have not been considered in the models: (1) longitudinal mass flow (perpendicular to the model cross section) coming from the higher eastern Guadalquivir Basin and (2) flow along the profile coming from the Internal Betics, which, despite having no direct isostatic effect on the basin, play an important role as a sediment source. A self-consistent analysis of the erosion/sedimentation balance could be better understood using a 3-D numerical approach explicitly incorporating surface transport processes over a wider region.

7. Conclusions

[53] The main conclusions arising from this work can be summarized as follows:

1. The kinematics of the Internal Betics and the Alborán Sea has no relevant isostatic effect on the subsidence of the Guadalquivir Basin. The formation of this basin is mostly related to thrust loading in the External Betics and to deeper loads probably related to lower crustal and lithospheric mantle thickness changes. The magnitude of this deeper load increases from zero beneath the northern limit of the present Guadalquivir Basin to 2.0×10^7 N m^{-2} (estimated error is $\pm 8 \times 10^6$ N m^{-2}) at a distance of 60 km to the SSE. This implies a mantle thickening derived from this load ranging between 20 and 41 km.

2. The equivalent elastic thickness of the lithosphere at the Guadalquivir Basin is T_e = 7–13 km (laterally increasing from east to west), whereas the thickness of the mechanical lithosphere and the thermal lithosphere are 53 km and 93 km, respectively.

3. These low T_e values can be reconciled with the lithospheric stratification, assuming mechanical decoupling between crust and mantle in the southern edge of Iberia. This mechanical decoupling may have acted as a detachment surface, explaining the strain partitioning between the crust and the lithospheric mantle suggested from this study and previous works.

4. Viscous stress relaxation and/or elastic-plastic stress limitation are required to explain the Guadalquivir Basin sediment geometry, assuming wedge progradation toward the foreland. Both anelastic processes can explain a reduction of the basin width during its formation and during periods of tectonic quiescence.

5. A substantial part of the present relief of Sierra Morena (a mountain range bounding the northern side of the basin) is related to flexural forebulge uplift.

[54] **Acknowledgments.** We want to express our gratitude to Xavier Berástegui and Carme Puig (Geological Survey, Barcelona) and to Contxita Taberner and José A. Gil (CSIC, Barcelona) for the interesting discussions that inspired this work. The manuscript has been enriched by constructive reviews by Mary Ford, Reini Zoetemeijer, and two anonymous reviewers. Financial support was granted by the European Union project Integrated Basin Studies (JOU2-CT92-0110).

References

Bakker, H. E., K. De Jong, H. Helmers, and C. Biermann, The geodynamic evolution of the Internal Zone of the Betic Cordilleras (SE Spain): A model based on structural analysis and geothermobarometry, *J. Metamorph. Geol.*, *7*(3), 359–381, 1989.

Balanyá, J. C., and V. Garčía-Dueñas, Les directions structurales dans le Domaine d'Alboran de part et d'outre du Detroit de Gibraltar, *C. R. Acad. Sci., Ser. II*, *304*, 929–933, 1987.

Balanyá, J. C., V. Garčía-Dueñas, J. M. Azanon, and M. Sanchez-Gomez, Alternating contractional and extensional events in the Alpujarride nappes of the Alborán Domain (Betics, Gibraltar Arc), *Tectonics*, *16*(2), 226–238, 1997.

Banks, C. J., and J. Warburton, Mid-crustal detachment in the Betic system of southeast Spain, *Tectonophysics*, *191*, 275–289, 1991.

Beaumont, C., Foreland basins, *Geophys. J. R. Astron. Soc.*, *65*, 291–329, 1981.

Berástegui, X., C. J. Banks, C. Puig, C. Taberner, D. Waltham, and M. Fernàndez, Lateral diapiric emplacement of Triassic evaporites at the southern margin of the Guadalquivir basin, Spain, *Geol. Soc. Spec. Publ.*, *134*, 49–68, 1998.

Bodine, J. H., M. S. Steckler, and A. B. Watts, Observations of flexure and the rheology of the oceanic lithosphere, *J. Geophys. Res.*, *86*, 3695–3707, 1981.

Bott, M. H. P., Sublithospheric loading and plate-boundary forces, *Philos. Trans. R. Soc. London*, *337*, 83–93, 1991.

Buiter, S. J. H., M. J. R. Wortel, and R. Govers, The role of subduction in the evolution of the Apennines foreland basin, *Tectonophysics*, *296*, 249–268, 1998.

Brunet, M. F., The influence of the evolution of the Pyrenees on adjacent basins, *Tectonophysics*, *129*, 343–354, 1986.

Burgess, P. L., and L. N. Moresi, Modeling rates and distribution of subsidence due to dynamic topography over subducting slabs: Is it possible to identify dynamic topography from ancient strata?, *Basin Res.*, *11*, 305–314, 1999.

Burov, E. B., and M. Diament, Flexure of the continental lithosphere with multilayered rheology, *Geophys. J. Int.*, *109*, 449–468, 1992.

Burov, E. B., and M. Diament, The effective elastic thickness (T_e) of continental lithosphere: What does it really mean?, *J. Geophys. Res.*, *100*, 3905–3927, 1995.

Calvert, A., E. Sandvol, D. Seber, M. Barazangi, S. Roecker, T. Mourabit, F. Vidal, G. Alguacil, and N. Jabour, Geodynamic evolution of the lithosphere and upper mantle beneath the Alboran region of the western Mediterranean: Constraints from travel time tomography, *J. Geophys. Res.*, *105*, 10,871–10,898, 2000.

Chapman, M. E., Techniques for interpretation of geoid anomalies, *J. Geophys. Res.*, *84*, 3793–3801, 1979.

Cloetingh, S., E. Burov, and A. Poliakov, Lithospheric folding: Primary response to compression? (from central Asia to Paris basin), *Tectonics*, *18*(6), 1064–1083, 1999.

Cloetingh, S., E. Burov, B. Andeweg, F. Beekmann, P. A. M. Andriessen, D. Garcia-Castellanos, G. de Vicente, and R. Vegas, Lithospheric folding in Iberia, *Tectonics*, 10.1029/2001TC901031, in press, 2002.

Comas, M. C., V. García-Dueñas, and M. J. Jurado, Neogene tectonic evolution of the Alboran Basin from MCS data, *Geo. Mar. Lett.*, *12*, 144–149, 1992.

Crampton, S. L., and P. A. Allen, Recognition of forebulge unconformities associated with early stage foreland basin development: Example from the North Alpine foreland basin, *AAPG Bull.*, *79*(10), 1495–1514, 1995.

Davis, D., J. Suppe, and F. A. Dahlen, Mechanics of fold-and-thrust belts and accretionary wedges, *J. Geophys. Res.*, *88*, 1153–1172, 1983.

Dewey, J. F., M. L. Helman, E. Turco, D. H. W. Hutton, and S. D. Knott, Kinematics of the western Mediterranean, in *Alpine Tectonics*, edited by M. P. Coward, D. Dietrich, and D. G. Park, *Geol. Soc. Spec. Publ.*, *45*, 265–283, 1989.

Fernàndez, M., X. Berástegui, C. Puig, D. Garčía-Castellanos, M. J. Jurado, M. Torné, and C. Banks, Geophysical and geological constraints on the evolution of the Guadalquivir foreland basin, Spain, in *Cenozoic Foreland Basins of Western Europe*, edited by A. Mascle et al., *Geol. Soc. Spec. Publ.*, *134*, 29–48, 1998a.

Fernàndez, M., I. Marzán, A. Correia, and E. Ramalho, Heat flow, heat production, and lithospheric thermal regime in the Iberian Peninsula, *Tectonophysics*, *291*, 29–53, 1998b.

Flemings, P. B., and T. E. Jordan, A synthetic stratigraphic model of foreland basins development, *J. Geophys. Res.*, *94*, 3851–3866, 1989.

Ford, M., W. H. Lockorish, and N. J. Kusznir, Tertiary foreland sedimentation in the Southern Subalpine Chains, SE France: A geodynamic appraisal, *Basin Res.*, *11*, 315–336, 1999.

Galindo Zaldivar, J., F. González Lodeiro, and A. Jaba-

loy, Progressive extensional shear structures in a detachment contact in the western Sierra Nevada (Betic Cordilleras, Spain), *Geodyn. Acta*, *3*, 73–85, 1989.

Garcia-Castellanos, D., Desarrollo de modelos numéricos de flexión litosférica: Aplicación a cuencas de antepaís y fosas oceánicas, Ph.D. thesis, Univ. de Barcelona, Barcelona, Spain, 1998.

Garcia-Castellanos, D., M. Fernández, and M. Torne, Numerical modeling of foreland basin formation: A program relating thrusting, flexure, sediment geometry and lithosphere rheology, *Comput. Geosci.*, *23*(9), 993–1003, 1997.

Garcia-Castellanos, D., M. Torne, and M. Fernàndez, Slab pull effects from a flexural analysis of the Tonga and Kermadec Trenches (Pacific Plate), *Geophys. J. Int.*, *141*, 479–484, 2000.

Garčía-Dueñas, V., and J. C. Balanyá, Fallas normales de bajo ángulo a gran escala en las Béticas Occidentales, *Geogaceta*, *9*, 33–37, 1991.

Garčía-Dueñas, V., J. C. Balanyá, and J. M. Martínez-Martínez, Miocene extensional detachments in the outcropping basement of the northern Alborán Basin (Betics) and their tectonic implications, *Geo. Mar. Lett.*, *12*, 88–95, 1992.

García-Hernández, M., A. C. López-Garrido, P. Rivas, and C. Sanz de Galdeano, Mesozoic palaeogeographic evolution of the external zones of the Betic Cordillera, *Geol. Mijnbouw*, *59*(2), 155–168, 1980.

González, A., D. Córdoba, R. Vegas, and L. M. Matias, Seismic crustal structure in the southwest of the Iberian Peninsula and the Gulf of Cadiz, *Tectonophysics*, *296*, 317–331, 1998.

Haq, B. U., J. Hardenbol, and P. R. Vail, Chronology of fluctuating sea levels since the Triassic, *Science*, *235*, 1156–1167, 1987.

Herraiz, M., G. De Vicente, R. Lindo, and J. G. Sánchez-Cabanero, Seismotectonics of the Sierra Albarrana area (southern Spain): Constraints for a regional model of the Sierra Morena-Guadalquivir Basin limit, in *Dynamics of Extensional Basins and Inversion Tectonics*, edited by S. Cloetingh et al., *Tectonophysics*, *266*, 425–442, 1996.

Lynch, H. D., and P. Morgan, The tensile strength of the lithosphere and the localization of extension, in *Continental Extension Tectonics*, edited by M. P. Coward, J. F. Dewey, and P. L. Hancock, *Geol. Soc. Spec. Publ.*, *28*, 53–65, 1987.

Lyon-Caen, H., and P. Molnar, Constraints on the structure of the Himalaya from an analysis of gravity anomalies and a flexural model of the lithosphere, *J. Geophys. Res.*, *88*, 8171–8191, 1983.

Lyon-Caen, H., and P. Molnar, Gravity anomalies, flexure of the Indian plate, and the structure, support, and evolution of the Himalaya and Ganga basin, *Tectonics*, *4*(6), 513–538, 1985.

Marzán, I., M. Fernàndez, and J. Cabal, Estudio geotérmico en la mitad Occidental de España, *Geogaceta*, *20*, 745–748, 1996.

McNutt, M. K., M. Diament, and M. G. Kogan, Variations of elastic plate thickness at continental thrust belts, *J. Geophys. Res.*, *93*, 8825–8838, 1988.

Monié, P., J. Galindo-Zaldívar, R. González Lodeiro, B. Goffé, and A. Jabaloy, $^{40}Ar/^{39}Ar$ geochronology of Alpine tectonism in the Betic Cordilleras (southern Spain), *J. Geol. Soc. London*, *148*, 289–297, 1991.

Montenat, C., and P. O. D'Estevou, Late Neogene basins evolving in the Eastern Betic transcurrent fault zone: An illustrated review, in *Tertiary Basins of Spain: The Stratigraphic Record of Crustal Kinematics*, edited by P. Friend and C. J. Dabrio, pp. 372–386, Cambridge Univ. Press, New York, 1996.

Mueller, S., L. C. George, and W. Spence, Inelastic models of lithospheric stress, I, Theory and application to outer-rise deformation, *Geophys. J. Int.*, *125*, 39–53, 1996a.

Mueller, S., W. Spence, and L. C. George, Inelastic models of lithospheric stress, II, Implications for outer-rise seismicity and dynamics, *Geophys. J. Int.*, *125*, 54–72, 1996b.

Mulugeta, G., Modeling the geometry of Coulomb thrust wedges, *J. Struct. Geol.*, *10*(8), 847–859, 1988.

Nadai, A., *Theory of Flow and Fracture of Solids*, vol. 2, 705 pp., McGraw-Hill, New York, 1963.

Perconig, E., Sur la constitution géologique de l'Andalousie Occidentale en particulier du Bassin du Guadalquivir (Espagne méridionale), in *Livre Mémoir du Professor Paul Fallot*, pp. 229–256, Soc. Géol. de Fr., Paris, 1962.

Perconig, E., Sobre la edad de la transgresión del Terciario Marino en el borde meridional de la Meseta, paper presented at I Congreso Hispano-Luso-Americano de Geoloğía Económica, I, Madrid, 1971.

Platt, J. P., Comment on "Alternating contractional and extensional events in the Alpujarride nappes of the Alboran Domain (Betics, Gibraltar Arc) by Balanya et al.", *Tectonics*, *17*(6), 973–976, 1998.

Platt, J. P., and R. L. Vissers, Extensional collapse of thickened continental lithosphere: A working hypothesis of the Alboran Sea and the Gibraltar Arc, *Geology*, *17*, 540–543, 1989.

Platt, J., S. Allerton, A. Kirker, and E. Platzman, Origin of the western Subbetic arc (S. Spain): Palaeomagnetic and structural evidence, *J. Struct. Geol.*, *17*, 765–775, 1995.

Platzman, E. S., Palaeomagnetic rotations and kinematics of the Gibraltar Arc, *Geology*, *20*, 311–314, 1992.

Platzman, E. S., J. P. Platt, and P. Olivier, Palaeomagnetic rotations and fault kinematics in the Rif arc of Morocco, *J. Geol. Soc. London*, *150*, 707–718, 1993.

Royden, L. H., Flexural behavior of the continental lithosphere in Italy: Constraints imposed by gravity and deflection data, *J. Geophys. Res.*, *93*, 7747–7766, 1988.

Royden, L. H., The tectonic expression of slab pull at continental convergent boundaries, *Tectonics*, *12*(2), 303–325, 1993.

Royden, L., and G. D. Karner, Flexure of the continental lithosphere beneath Apennine and Carpathian foredeep basins: Evidence for an insufficient topographic load, *AAPG Bull.*, *68*, 704–712, 1984.

Sanz de Galdeano, C., Geologic evolution of the Betic Cordilleras in the western Mediterranean, Miocene to present, *Tectonophysics*, *172*, 107–119, 1990.

Sanz de Galdeano, C., and J. Rodŕíguez-Fernández, Neogene palaeogeography of the Betic Cordillera: an attempt at reconstruction, in *Tertiary Basins of Spain: The Stratigraphic Record of Crustal Kinematics*, edited by P. Friend and C. J. Dabrio, 323–329, Cambridge Univ. Press, New York, 1996.

Schlunegger, F., L. Werner, and A. Matter, Sedimentary sequences, seismic facies, subsidence analysis, and evolution of the Burdigalian Upper Marine Molasse Group, central Switzerland, *AAPG Bull.*, *81*, 1185–1207, 1997.

Seber, D., M. Baranganzi, A. Ibenbrahim, A. Demnati, and J. Civis, Geophysical evidence for lithospheric delamination beneath the Alboran Sea and Rif-Betic mountains, *Nature*, *379*, 785–790, 1996.

Sierro, F. J., J. A. González-Delgado, C. J. Dabrio, J. A. Flores, and J. Civis, Late Neogene depositional sequences in the foreland basin of Guadalquivir (SW Spain), in *Tertiary Basins of Spain: The Stratigraphic Record of Crustal Kinematics*, edited by P. Friend and C. J. Dabrio, pp. 339–345, Cambridge Univ. Press, New York, 1996.

Sinclair, H. D., B. J. Coakley, P. A. Allen, and A. B. Watts, Simulation of foreland basin stratigraphy using a diffusion model of mountain belt uplift and erosion: An example from the central Alps, Switzerland, *Tectonics*, *10*(3), 599–620, 1991.

Stapel, G., The nature of isostasy in West Iberia, P.D. thesis, 148 pp., Vrije Univ., Amsterdam, 1999.

Stewart, J., and A. B. Watts, Gravity anomalies and spatial variations of flexural rigidity at mountain ranges, *J. Geophys. Res.*, *102*, 5253–5327, 1997.

Stockmal, G. S., C. Beaumont, and R. Boutilier, Geodynamic models of convergent margin tectonics: Transition from rifted margin to overthrust belt and consequences for foreland-basin development, *AAPG Bull.*, *70*, 181–190, 1986.

Talwani, M., J. L. Worzel, and M. Landisman, Rapid Gravity computations for two-dimensional bodies with application to the Mendocino Submarine Fracture zone, *J. Geophys. Res.*, *64*, 49–59, 1959.

Torne, M., and E. Banda, Crustal thinning from the Betic Cordillera to the Alboran Sea, *Geo. Mar. Lett.*, *12*, 76–81, 1992.

Torne, M., M. Fernàndez, M. C. Comas, and J. I. Soto, Lithospheric structure beneath the Alboran Basin: Results from 3D gravity modeling and tectonic relevance, *J. Geophys. Res.*, *105*, 3209–3228, 2000.

Toth, J., N. J. Kusznir, and S. S. Flint, A flexural isostatic model of lithospheric shortening and foreland basin formation: Application to the Eastern Cordillera and Subandean belt of NW Argentina, *Tectonics*, *15*, 213–223, 1996.

Tubia, J. M., and J. L. Gil-Ibarguchi, Eclogites of the Ojen nappe: A record of subduction in the Alpujarride complex (Betic Cordilleras, southern Spain), *J. Geol. Soc. London*, *148*, 801–804, 1991.

Van der Beek, P. A., and S. Cloetingh, Lithospheric flexure and the tectonic evolution of the Betic cordilleras (SE Spain), *Tectonophysics*, *203*, 325–344, 1992.

Van Wees, J. D., and S. Cloetingh, A finite-difference technique to incorporate spatial variations in rigidity and planar faults into 3-D models for lithospheric flexure, *Geophys. J. Int.*, *117*, 179–195, 1994.

Vissers, R. L., J. P. Platt, and D. Van der Wal, Late orogenic extension of the Betic Cordillera and the Alboran Domain: A lithospheric view, *Tectonics*, *14*, 786–803, 1995.

Waschbusch, P. J., and L. H. Royden, Spatial and temporal evolution of foredeep basins: Lateral strength variations and inelastic yielding in continental lithosphere, *Basin Res.*, *4*, 179–195, 1992.

Watts, A. B., The elastic thickness of the lithosphere and the evolution of foreland basins, *Basin Res.*, *4*, 169–178, 1992.

Zeck, H. P., P. Monier, I. M. Villa, and B. T. Hansen, Very high rates of cooling and uplift in the Alpine belt of the Betic Cordilleras, southern Spain, *Geology*, *20*, 79–82, 1992.

M. Fernàndez and M. Torne, Institute of Earth Sciences Jaume Alme (CSIC), Solé i Sabarís s/n, 08028 Barcelona, Spain. (mfernandez@ija.csic.es; mtorne@ija.csic.es)

D. Garcia-Castellanos, Faculty of Earth Sciences, Vrije Universiteit, De Boelelaan, 1085, NL-1081 HV Amsterdam, Netherlands. (gard@geo.vu.nl)